Pré-Publicações do Departamento de Matemática
Universidade de Coimbra
Preprint Number 08–18

LONGITUDINAL DISPERSION IN A HORIZONTAL SUBSURFACE FLOW CONSTRUCTED WETLAND: A NUMERICAL SOLUTION

ADÉRITO ARAÚJO, ERCÍLIA SOUSA AND ANTÓNIO ALBUQUERQUE

ABSTRACT: We present a numerical solution for the dead zone model which describes the solute transport in a subsurface and horizontal flow constructed wetland. This model is a system of two mass balance equations for two conceptual areas: the main channel and the storage zone. We use finite difference schemes to determine the numerical solution of the system and we study its convergence by presenting properties related to the stability and accuracy of the schemes.

Concerning the experimental results, the magnitude of the longitudinal dispersion and the extension of dead volumes is estimated for clean conditions and after a certain operating period under organic loading conditions. The results showed a considerable amount of longitudinal dispersion through the bed, which was very strong near the feeding point, indicating the occurrence of mixing and significant presence of dead zones and short-circuiting.

KEYWORDS: Finite differences; dead zone model; constructed wetland; hydrodynamic characteristics.

1. Introduction

Constructed wetlands are considered a technical, economical and environmental sustainable solution for wastewater treatment in small communities since they present a good efficiency on pollutant removal and high filter capacity. Constructed treatment wetland with transient storage can be found in literature such as, in [4], [5]. The most used solution presented a subsurface and horizontal flow bed (SSHF) and it is recognized to have a good ecological integration. However, the packing media used as bed it may become frequently clogged due to factors whose interrelations are not well known. The transport of solutes in the bed is, therefore, difficult to study since there are many factors which may affect the transport mechanisms, such as the development of roots, media characteristics (e.g. type of material, porosity and physical properties such as sorption), excessive biofilm growth, hydraulic and organic loadings, chemical and biochemical transformations and accumulation of solids.

Received April 4, 2008.

A complex interaction of these processes in the porous media may stimulate the development of immobile areas, dead volumes, hydraulic short-circuiting, internals recirculation and changes in dispersion conditions, which may affect the solute distribution through media and, therefore, the treatment efficiency may be negatively affected. The analysis of flow patterns for different bed characteristics (e.g. with and without vegetation) and organic loadings is essential for a better understanding of the transport of solutes in such systems and, therefore, to allow accurate prediction of treatment. A reliable mean of evaluating the extension of those mechanisms is to carry out tracer tests through the bed and analyse the exit concentration curves with time (breakthrough curve) through numerical solutions of transport equations. The hydrodynamic characteristics of the bed, in terms of flow regime, extension of dead areas and longitudinal dispersion may be analysed by estimating parameters such as the Peclet number or the ratio of dead zones volumes. Therefore, the objective of this paper is to propose a numerical solution for the dead zone model to simulate the solute transport in a SSHF constructed wetland.

Analysis and simulation of longitudinal solute transport in porous media require consideration of the main physical mechanisms and processes, i.e, advection diffusion/dispersion and transient storage. The dead zone model is a system of two mass balance equations for two conceptual areas: the main channel and the storage zone. The main channel is defined as that portion of the stream in which advection and dispersion are the dominant transport mechanisms. The storage zone is defined as the portion of the stream that contributes to transient storage. Within the main channel, solutes are transported downstream by advection and dispersion. Advection and dispersion are not included in the storage zones, where downstream transport is negligible.

To determine the numerical solution we use finite difference schemes and in the end of the paper we analyse its convergence through stability and accuracy. The magnitude of the longitudinal dispersion (Pe) and the extension of dead volumes (ϵ) will also be estimated for clean conditions and after an operating period of eight months under organic loading conditions.

2. Model for estimating hydrodynamic characteristics

For a conservative solute the equations governing longitudinal transport and mixing in a stream without lateral inflow can be written as follows (see e.g. [2], [7])

$$\frac{\partial C}{\partial t} + \frac{Q}{A}\frac{\partial C}{\partial x} = AD\frac{\partial^2 C}{\partial x^2} + \epsilon T^{-1}(C_s - C), \tag{1}$$

$$\frac{\partial C_s}{\partial t} = T^{-1}(C - C_s), \tag{2}$$

with C and C_s as solute concentration (mg/l) in main stream and storage zones, Q denotes flow rate (m^3/h), A flow cross-section m^2, D the dispersion coefficient (m^2/h) and ϵ the dimensionless ratio of dead zone volume and main volume per unit length. T is an exchange parameter (h) related to mean dead zone residence time. The later two parameters can be expressed as

$$\epsilon = \frac{A_s}{A} \quad \text{and} \quad T^{-1} = \alpha\frac{A}{A_s},$$

with A_s denoting the storage zone cross-sectional area (m^2) and α the storage zone exchange coefficient (h^{-1}).

For transport and mixing in a uniform reach with the steady flow, this system reduces to [6]

$$\frac{\partial C}{\partial t} + u\frac{\partial C}{\partial x} = D\frac{\partial^2 C}{\partial x^2} + \epsilon T^{-1}(C_s - C), \tag{3}$$

$$\frac{\partial C_s}{\partial t} = T^{-1}(C - C_s), \tag{4}$$

with u the mean effective flow velocity (m/h).

For our particular problem the initial conditions are given by

$$C(x,0) = 0 \quad \text{and} \quad C_s(x,0) = 0 \quad \text{for} \quad x > 0. \tag{5}$$

Although in most of the experimental procedures there are some uncertainty about what happens at the upstream boundary, that is, near the tracer injection point we evaluate it as a function

$$C(0,t) = g(t), \quad t > 0. \tag{6}$$

The boundary condition, $g(t)$, represents the solute concentration at the inflow boundary and is given by the following exponential decay

$$g(t) = C_0 \mathrm{e}^{-Qt/V_i}, \tag{7}$$

where V_i denotes the volume of injected tracer, C_0 is the concentrated solution injected at the beginning and Q (l/h) denotes the flow rate.

This condition is obtained considering that the inflow concentration is governed by the differential equation,

$$\frac{dg}{dt} = -\frac{Q}{V_i} g, \quad \text{with} \quad g(0) = C_0,$$

which describes the inflow decay by a rate of Q/V_i.

3. Finite differences discretization

To derive a finite difference scheme we suppose there are approximations $C^n := \{C_i^n\}$ to the values $C(x_i, t_n)$ and ${C_s}^n := \{C_{s,i}^n\}$ to the values $C_s(x_i, t_n)$ at the mesh points

$$x_i = i\Delta x, \ i = 0, 1, 2, \ldots, N.$$

If we choose a uniform space step Δx and time step Δt, there are two dimensionless quantities very important in the properties of a numerical scheme

$$\nu = \frac{u\Delta t}{\Delta x} \qquad \mu = \frac{D\Delta t}{(\Delta x)^2}.$$

The quantity ν is usually called the Courant (or CFL) number and μ is called the Fourier number.

We use the usual central and second difference operators,

$$\Delta_0 C_i^n := \frac{1}{2}(C_{i+1}^n - C_{i-1}^n) \text{ and } \delta^2 C_i^n := C_{i+1}^n - 2C_i^n + C_{i-1}^n$$

to describe the finite difference schemes.

Using second-order centered finite differences operators in space and the trapezoidal rule in time (Crank-Nicolson scheme), we obtain

$$\begin{aligned} \frac{C_i^{n+1} - C_i^n}{\Delta t} &= \frac{1}{2}\left(-\frac{u}{\Delta x}\Delta_0 C_i^{n+1} + \frac{D}{\Delta x^2}\delta^2 C_i^{n+1} + \epsilon T^{-1}(C_{s,i}^{n+1} - C_i^{n+1})\right) \\ &\quad + \frac{1}{2}\left(-\frac{u}{\Delta x}\Delta_0 C_i^n + \frac{D}{\Delta x^2}\delta^2 C_i^n + \epsilon T^{-1}(C_{s,i}^n - C_i^n)\right), \end{aligned} \tag{8}$$

$$\frac{C_{s,i}^{n+1} - C_{s,i}^n}{\Delta t} = \frac{1}{2}T^{-1}(C_i^{n+1} - C_{s,i}^{n+1}) + \frac{1}{2}T^{-1}(C_i^n - C_{s,i}^n). \tag{9}$$

In order to avoid implicitness we use the decoupling procedure of the two equations suggested in [7]. First we rearrange the terms in (9) in the form

$$C_{s,i}^{n+1} = (1-2\gamma)C_{s,i}^{n} + \gamma(C_i^n + C_i^{n+1}), \tag{10}$$

where

$$\gamma = \frac{\Delta t}{2T+\Delta t}.$$

Note that $\gamma < 1$. Secondly, replacing (10) in (8), we obtain

$$\begin{aligned} C_i^{n+1} &= C_i^n + \frac{1}{2}\left(-\nu\Delta_0 + \mu\delta^2 - \Delta t\epsilon T^{-1}(1-\gamma)\right) C_i^{n+1} \\ &\quad + \frac{1}{2}\left(-\nu\Delta_0 + \mu\delta^2 - \Delta t\epsilon T^{-1}(1-\gamma)\right) C_i^n + \Delta t\epsilon T^{-1}(1-\gamma)C_{s,i}^n. \end{aligned} \tag{11}$$

Since $\Delta t\epsilon T^{-1}(1-\gamma) = 2\epsilon\gamma$, we may write the system (10)–(11) in the form

$$aC_i^{n+1} = bC_i^n + dC_{s,i}^n, \tag{12}$$

$$C_{s,i}^{n+1} = (1-2\gamma)C_{s,i}^n + \gamma(C_i^n + C_i^{n+1}), \tag{13}$$

where $d = 2\epsilon\gamma$ and a and b are the difference operators

$$a = 1 - \frac{1}{2}\left(-\nu\Delta_0 + \mu\delta^2 - 2\epsilon\gamma\right), \quad b = 1 + \frac{1}{2}\left(-\frac{\nu}{2}\Delta_0 + \mu\delta^2 - 2\epsilon\gamma\right).$$

We can write our numerical method in the matricial form

$$\mathbf{M}_1\mathbf{C}^{n+1} = \mathbf{M}_2\mathbf{C}^n + \mathbf{v}^n, \tag{14}$$

where $\mathbf{C}^n = (C^n, C_s^n)$ and $\mathbf{v}^n$ is a vector that contains the boundary values. The matrices $\mathbf{M}_1$ and $\mathbf{M}_2$ are defined by

$$\mathbf{M}_1 = \begin{bmatrix} N_1 & 0 \\ -\gamma I & I \end{bmatrix} \quad \text{and} \quad \mathbf{M}_2 = \begin{bmatrix} N_2 & dI \\ \gamma I & (1-2\gamma)I \end{bmatrix},$$

where I is the identity matrix of order $N-1$,

$$N_1 = I - \frac{1}{2}(-\nu D_c + \mu D_2 - 2\epsilon\gamma), \quad N_2 = I + \frac{1}{2}\left(-\frac{\nu}{2}D_c + \mu D_2 - 2\epsilon\gamma\right)$$

and D_c and D_2 the tridiagonal matrices of order $N-1$ such that

$$D_c = \text{Tridiag}(-1,0,1), \quad \text{and} \quad D_2 = \text{Tridiag}(1,-2,1).$$

The matricial form can also de written in the explicit form,

$$\mathbf{C}^{n+1} = \mathbf{M}_1^{-1}\mathbf{M}_2\mathbf{C}^n + \mathbf{M}_1^{-1}\mathbf{v}^n, \tag{15}$$

where $\mathbf{M}_1^{-1} = \begin{bmatrix} N_1^{-1} & 0 \\ \gamma N_1^{-1} & I \end{bmatrix}$.

4. Convergence of the finite difference scheme

In order to study the convergence of the finite difference scheme (8)–(9), we will consider the so-called method of lines approach. In this approach the solution process is thought of as consisting of two parts: the space discretization and the time integration. According to Verwer and Sanz-Serna [9], to prove the convergence we need to establish the consistency and stability of both spatial and time discretisations.

4.1. Consistency. We will perform a traditional consistent argument [8]. Let $v = v(x,t)$ and $v_s = v_s(x,t)$ be the solutions to our system of equations. We denote by τ_i^n and $\tau_{s,i}^n$ the truncation errors associated with the equations (3) and (4) respectively. We have

$$\begin{aligned}\tau_i^n &= \frac{v_i^{n+1} - v_i^n}{\Delta t} - \frac{1}{2}\left(-\frac{u}{\Delta x}\Delta_0 v_i^{n+1} + \frac{D}{\Delta x^2}\delta^2 v_i^{n+1}\right) \\ &\quad -\frac{1}{2}\left(-\frac{u}{\Delta x}\Delta_0 v_i^{n} + \frac{D}{\Delta x^2}\delta^2 v_i^{n}\right) + \frac{1}{2}\epsilon T^{-1}(v_{s,i}^{n+1} + v_{s,i}^n) + \frac{1}{2}\epsilon T^{-1}(v_i^{n+1} + v_i^n)\end{aligned}$$

and

$$\tau_{s,i}^n = \frac{v_{s,i}^{n+1} - v_{s,i}^n}{\Delta t} - \frac{1}{2}T^{-1}(v_{s,i}^{n+1} + v_{s,i}^n) - \frac{1}{2}T^{-1}(v_i^{n+1} + v_i^n)$$

Therefore

$$\begin{aligned}\tau_i^n &= \left(\frac{\partial v}{\partial t}\right)_i^{n+1/2} + \mathcal{O}(\Delta t^2) - u\left(\frac{\partial v}{\partial x}\right)_i^{n+1/2} + D\left(\frac{\partial^2 v}{\partial x^2}\right)_i^{n+1/2} + \mathcal{O}(\Delta x^2) \\ &\quad + \mathcal{O}(\Delta t^2) + \epsilon T^{-1}(v_s - v)_i^{n+1/2} + \mathcal{O}(\Delta x^2)\end{aligned}$$

and

$$\tau_{s,i}^n = \left(\frac{\partial v}{\partial t}\right)_i^{n+1/2} + \mathcal{O}(\Delta t^2) - T^{-1}(v - v_s)_i^{n+1/2} + \mathcal{O}(\Delta t^2)$$

The scheme is accurate of order $\mathcal{O}(\Delta t^2) + \mathcal{O}(\Delta x^2)$. Part of the $\mathcal{O}(\Delta t^2)$ terms on the first equation depend on the source term v_s. Therefore a lost of order can come from the source term v_s. We could approximate v_s by $(v_s)_i^{n+1/2}$ instead of $(v_{s,i}^{n+1} + v_{s,i}^n)/2$ and the resulting scheme would be just as good (same order) or better (no order terms due to v_s on the first equation). But in this case, this would interfere with the second differential equation.

Note that for $\epsilon = 0$ and by the rearrangement of the terms obtained by Taylor's expansion the expression for the local truncation error is given by

$$\tau_i^n = \left(\frac{u}{6}\Delta x^2 + \frac{u^3}{12}\Delta t^2\right)\frac{\partial^3 v}{\partial x^3} + \mathcal{O}^3(\Delta x, \Delta t).$$

4.2. Stability. We consider the problem (3)–(4) written in the form

$$\frac{\partial \mathbf{C}}{\partial t} + \mathbf{U}\frac{\partial \mathbf{C}}{\partial x} = \mathbf{D}\frac{\partial^2 C}{\partial x^2} + \mathbf{E}\mathbf{C}, \tag{16}$$

where $\mathbf{C}$ represents the exact solution $\mathbf{C}(x,t) = (C(x,t), C_s(x,t))$ and

$$\mathbf{U} = \begin{bmatrix} u & 0 \\ 0 & 0 \end{bmatrix}, \quad \mathbf{D} = \begin{bmatrix} D & 0 \\ 0 & 0 \end{bmatrix} \quad \text{and} \quad \mathbf{E} = T^{-1}\begin{bmatrix} -\epsilon & \epsilon \\ 1 & -1 \end{bmatrix}. \tag{17}$$

The stability of the spatial discretization is based on the existence of a bounded logarithmic matrix norm [3]. The concept of C-stability, which is linked with stability in the Lax-Richtmyer sense [3], is employed for deciding upon the stability for the time integration.

Let us first consider the spatial discretization. The semi-discrete system of ordinary differential equations (16)–(17) may be written in the form

$$\frac{d\mathbf{C}}{dt} = \mathbf{M}\mathbf{C},$$

where $\mathbf{C}$ now represents the solution at the discrete points, that is, $\mathbf{C}(x_i,t) = (C(x_i,t), C_s(x_i,t))$. The matrix $\mathbf{M}$ is given by

$$\mathbf{M} = \frac{1}{2\Delta x}D_c \otimes \mathbf{U} + \frac{1}{\Delta x^2}D_2 \otimes \mathbf{D} + I \otimes \mathbf{E},$$

where $\otimes$ denotes the Kronecker product [3]. Since this discretization is of second order and therefore consistent with our problem, to prove the convergence of the spatial discretization we just need to prove the existence of a constant μ_{max} which is independent of the grid spacing and such that

$$\mu_{max} \geq \mu_\infty[\mathbf{M}],$$

where $\mu_\infty[\cdot]$ is a logarithmic matrix norm associated with the infinity norm and is given by,

$$\mu_\infty[\mathbf{M}] = \max_i \left(a_{ii} + \sum_{j \neq i} |a_{ij}| \right).$$

According to the structure of the matrix $\mathbf{M}$, we may easily conclude that

$$\mu_\infty[\mathbf{M}] = \max \left\{ \left| \frac{u}{2\Delta x} + \frac{D}{\Delta x^2} \right| - \frac{2D}{\Delta x^2} + \left| -\frac{u}{2\Delta x} + \frac{D}{\Delta x^2} \right| \right\}.$$

Note that, if

$$\frac{u\Delta x}{D} > 2,$$

then $\mu_\infty[\mathbf{M}] = \mu_{max} = 0$. Otherwise, $\mu_\infty[\mathbf{M}] \leq \mu_{max} = u^2 D$. Then $\mu_\infty[\mathbf{M}]$ is bounded and we can conclude that the spatial discretization is convergent.

For the time integration we consider the Crank-Nicholson scheme

$$\mathbf{C}^{n+1} = \mathbf{C}^n + \frac{\Delta t}{2} \mathbf{M} \left(\mathbf{C}^{n+1} + \mathbf{C}^n \right).$$

In order to establish the C-stability of this scheme we prove the existence of a positive real number $\Delta t_0 = \Delta t_0(\Delta x)$ and a real constant C_0, independent of Δt and Δx, such that for each $\Delta t \in]0, \Delta t_0]$ and each approximated solution $\mathbf{C}, \widetilde{\mathbf{C}}$

$$\|\widetilde{\mathbf{C}}^{n+1} - \mathbf{C}^{n+1}\|_\infty \leq (1 + C_0 \Delta t) \|\widetilde{\mathbf{C}}^n - \mathbf{C}^n\|_\infty.$$

Let $(\mathbf{C}^n, \mathbf{C}^{n+1})$ and $(\widetilde{\mathbf{C}}^n, \widetilde{\mathbf{C}}^{n+1})$ denote two solution pairs of the Crank-Nicholson scheme, i.e.,

$$\mathbf{C}^{n+1} = \mathbf{C}^{n+1} + \frac{\Delta t}{2} \mathbf{M}(\mathbf{C}^n + \mathbf{C}^{n+1}),$$

$$\widetilde{\mathbf{C}}^{n+1} = \widetilde{\mathbf{C}}^n + \frac{\Delta t}{2} \mathbf{M}(\widetilde{\mathbf{C}}^n + \widetilde{\mathbf{C}}^{n+1}).$$

Then

$$(\mathbf{I} - \frac{\Delta t}{2} \mathbf{M})(\widetilde{\mathbf{C}}^{n+1} - \mathbf{C}^{n+1}) = (\mathbf{I} - \frac{\Delta t}{2} \mathbf{M})(\widetilde{\mathbf{C}}^n - \mathbf{C}^n).$$

By applying the infinity norm, $|| \cdot ||_\infty$, and using the properties of the logarithmic norm [3], we obtain

$$\|\widetilde{\mathbf{C}}^{n+1} - \mathbf{C}^{n+1}\|_\infty \leq \left(\frac{2 + \Delta t \mu_{max}}{2 - \Delta t \mu_{max}} \right) \|\widetilde{\mathbf{C}}^n - \mathbf{C}^n\|_\infty,$$

for $0 \leq \Delta t \mu_{max} < 2$.

Therefore, according to the results above we may conclude the following.

Theorem 1. *For $\frac{u\Delta x}{D} > 2$, the method (8)–(9) is unconditionally convergent. For $\frac{u\Delta x}{D} \leq 2$, the method is convergent if $\Delta t \leq \frac{2}{u^2 D}$.*

Note that, $u\Delta x/D$ is the mesh Peclet number. When the mesh Peclet number is less or equal to 2, the upper bound to the time step is a non-restrictive condition, since u and D are less than one.

It is worth remarking that, if we use upwinding for discretizing the first derivative, instead of using central differences, the bound for $\mu_\infty[\mathbf{M}]$ would be $\mu_{max} = 0$. In this case, for each $\Delta t \in]0, \Delta t_0]$,

$$\|\widetilde{\mathbf{C}}^{n+1} - \mathbf{C}^{n+1}\|_\infty \leq \|\widetilde{\mathbf{C}}^{n} - \mathbf{C}^{n}\|_\infty,$$

which is the definition of the numerical method being contractive for (16)–(17) with respect to the infinity norm. Additionally, if $\mathbf{C}^{n+1} = \mathbf{C}^n = \mathbf{0}$ is a solution of the numerical method for all $\Delta t > 0$, contractivity implies monotonocity, and so for all $\Delta t \in]0, \Delta t_0]$, $\|\mathbf{C}^{n+1}\|_\infty \leq \|\mathbf{C}^n\|_\infty$.

5. Materials and Methods

A laboratory SSHF system with 2.0 m $\times$ 0.80 m $\times$ 0.50 m was used to carry out two series of tracer tests at the mean flow velocity of 0.0047 m h^{-1} (11.3 cm d^{-1}). The submerged media was composed by gravel (0.20 m in depth and porosity of 0.4). Series I was executed with the bed without vegetation and Series II with the bed already colonized with Phragmites australis after an operation period of eight months at organic loads ranging from 10 to 33 g COD m^{-2} d^{-1} (roots were well developed and spread over the bed). Each Series included three assays with tap water and a quickly injection of 0.5 l of sodium chloride with a concentration of 100 g l^{-1} (C_0) for three bed lengths: Inlet-P2 (0.33 m), Inlet-P5 (1.00 m) and Inlet-P8 (1.93 m). The response was evaluated by online measurement of a conductivity TetraCon 325 probe and Multi 340i WTW meter (Figure 1). The time duration of each assay was up to 15 times the theoretical hydraulic retention time until no significant conductivity were observed at the measuring point.

6. Numerical solution versus experimental results

In this section we present the experimental results and the numerical solution which simulates the transport mechanism that occurs experimentally.

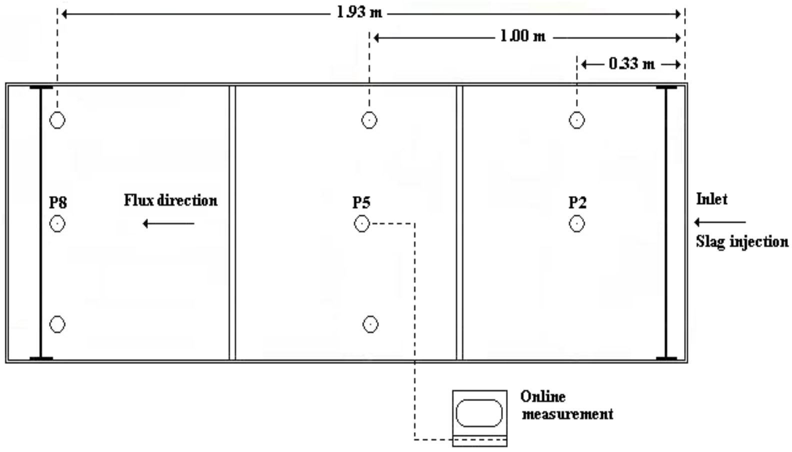

FIGURE 1. Schematic representation of the laboratory device (plant)

In Figures 2–4 we plot the experimental results versus the numerical solution of the system (12) and (13). These numerical results were obtained by adjusting the parameters ϵ, T, D and Pe to the experimental results, according to Table 1. Figures 5 to 7 show the numerical solution of the solute concentration in storage zones.

Assay	L	tfinal	ϵ	T	D	Pe	DaI
I.P2	0.33	100	15	1000	3.0×10^{-4}	5.6	1.04
I.P5	1.00	250	26	3650	3.0×10^{-4}	29.5	0.84
I.P8	1.93	500	25	6000	4.1×10^{-4}	41	0.96
II.P2	0.33	100	15	1300	1.4×10^{-4}	12	0.80
II.P5	1.00	250	26	5700	1.5×10^{-4}	50	0.63
II.P8	1.93	500	25	7000	2.8×10^{-4}	60	0.83

TABLE 1. Results for Series I and II

Using global parameter uncertainty analysis, Wagner and Harvey [10] showed that the experimental Damköhler number, DaI is a valuable indicator of the reliability of storage zone cross-sectional area and exchange coefficient estimates. The use of the experimental Damköhler number was adapted from similar subsurface transport research conducted by Bahr and Rubin [1]. The experimental Damköhler number is

$$DaI = \frac{\alpha(1 + A/A_s)L}{u} = \frac{T^{-1}\epsilon(1+\epsilon^{-1})L^2}{PeD} = \frac{(1+\epsilon)L^2}{TPeD},$$

where L is the flow path length and the Peclet number is given by $Pe = \frac{uL}{D}$. The experimental Damköhler numbers found from the transient storage modeling conducted here are listed in Table 1.

Wagner and Harvey [10] found parameter uncertainties to be lowest when DaI was on the order of 1.0 and concluded that parameters were well estimated when DaI was on the order of 0.1 to 10. When DaI values were much less than $1 (< 0.01)$, due to high velocity, large exchange time scale (α or A/A_s is small), and short flow-path length, parameter uncertainties are high because only a small amount of tracer interacts with storage zones over the length of the flow-path.

When DaI values are much greater than 1, solute exchange rates are high compared with the velocity, or the flow path is long. In such cases, most if not all solute undergoes some exchange into the storage zone and the storage zone parameters can only be estimated with large uncertainties. It can be seen in Table 1 that DaI values were found to be within acceptable limits.

Figures 2–4 show the results for the assays I.P2, I.P5, I.P8 in clean conditions and for the assays II.P2, II.P5, II.P8, after an operating period of eight months under organic loading conditions. Most of the times due to the fact that we are uncertain about what happens at the inflow boundary, the numerical solution is more difficult to adjust to the experimental results near the boundary. In our case the assays I.P2 and II.P2 are the closest ones to the boundary. Nevertheless the numerical solution seems to perform quite well for these cases.

The results show that the changes observed in the bed from Series I to Series II (the development of plants, roots and biofilm and the retention of solid material) did not seem to influence the hydrodynamic characteristics of the overall bed. A small amount of dispersion occurred (Pe between 40 and 60) and the flow regime was plug flow. However, it was observed a strong dispersion in the inlet section (Pe between 5 and 12). For clean conditions (I.P2), this circumstance may be explained by the occurrence of mixing and molecular diffusion (both longitudinal and axial) due to the closeness of the feeding point and the presence of a solute concentration gradient, respectively. The lower dispersion observed for the colonized bed (II.P2) seemed to be associated with the significant development of dead zones and the consequent occurrence of short-circuiting. The differences observed in D and Pe for clean and colonized conditions may be explained by spatial variations of the effective porosity after the bed colonization.

References

[1] Bahr JM, Rubin J, Direct comparison of kinetic and local equilibrium formulations for solute transport affected by surface reactions. *Water Resource Res.*, 1987, **23**(3):438-452.

[2] Bencala KE, Walters RA. Simulation of solute transport in a mountain pool-and-riffle stream: a transient storage model. *Water Resour Res*, 1983, **19**(3):718-724.

[3] Dekker K, Verwer JG, *Stability of Runge-Kutta Methods for Nonlinear Stiff Differential Equations*. CWI Monograph 2, Elsevier, Amsterdam, 1984.

[4] Keefe SH, Barber LB, Runkel RL, Ryan JN, McKnight DM, Wass RD, Conservative and reactive solute transport in constructed wetlands. *Water Resource Res.*, 2004, **40**: W01201, doi:10.1029/2003WR002130.

[5] Martinez CJ, Wise WR, Analysis of constructed treatment wetland hydraulics with the transient storage model OTIS. *Ecological Engineering*, 2003, **20**(3):211.

[6] Nordin CF, Troutman BM, Longitudinal dispersion in rivers: the persistence of skewness in observed data. *Water Resour Res* 1980 **16**(1):123-128.

[7] Runkel RL, Chapra SC, An efficient numerical solution of the transient storage equations for solute transport in small streams. *Water Resour Res*, 1993, **29**(1):211-215.

[8] Thomas JW *Numerical Partial Differential Equations: Finite Difference Methods*. Springer-Verlag, New York, 1995.

[9] Verwer, JG, Sanz-Serna JM, Convergence of Method of Lines Approximations to Partial Differential Equations. *Computing*, 1984, **33**(3-4):297-313.

[10] Wagner BJ, Harvey JW, Experimental design for estimating parameters of rate-limited mass transfer: analysis of stream tracer studies. *Water Resource Res.*, 1997, **33**(7):1731-1741.

Adérito Araújo
CMUC, Department of Mathematics, University of Coimbra, 3001-454 Coimbra, Portugal

Ercília Sousa
CMUC, Department of Mathematics, University of Coimbra, 3001-454 Coimbra, Portugal

António Albuquerque
C-MADE, Department of Civil Engineering and Architecture, University of Beira Interior, 6201-001 Covilha, Portugal

Solute concentration, C, in main stream

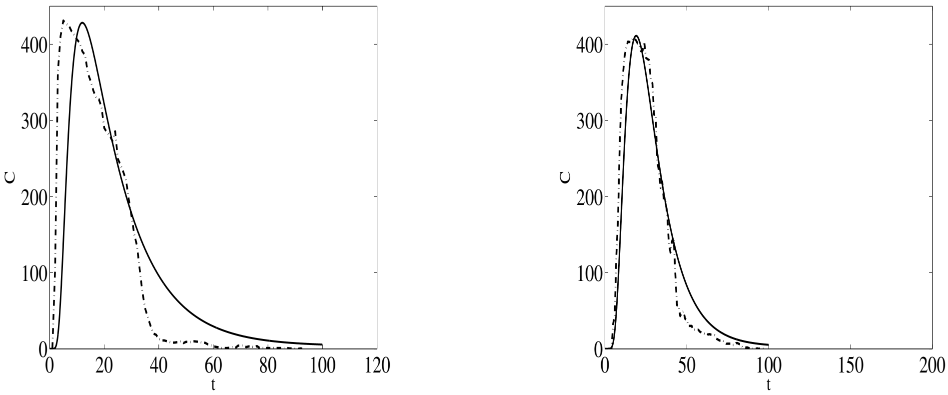

FIGURE 2. Numerical Solution (−); Experimental results (−·−): (a) I.P2 (b) II.P2

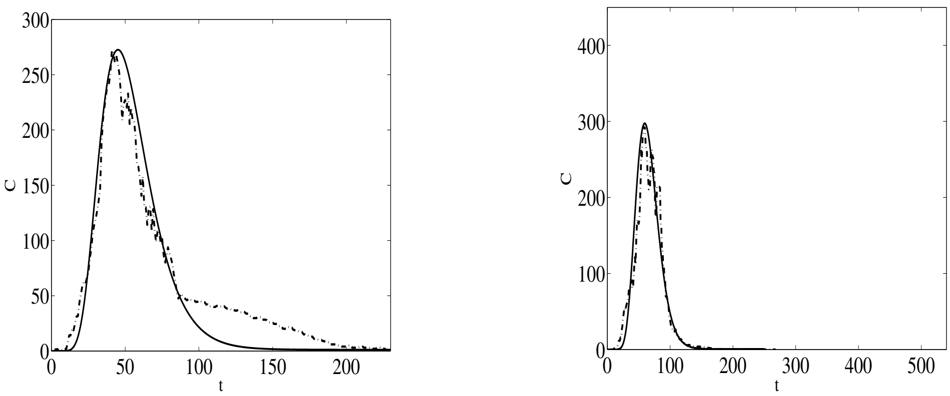

FIGURE 3. Numerical Solution (−); Experimental results (−·−): (a) I.P5 (b) II.P5

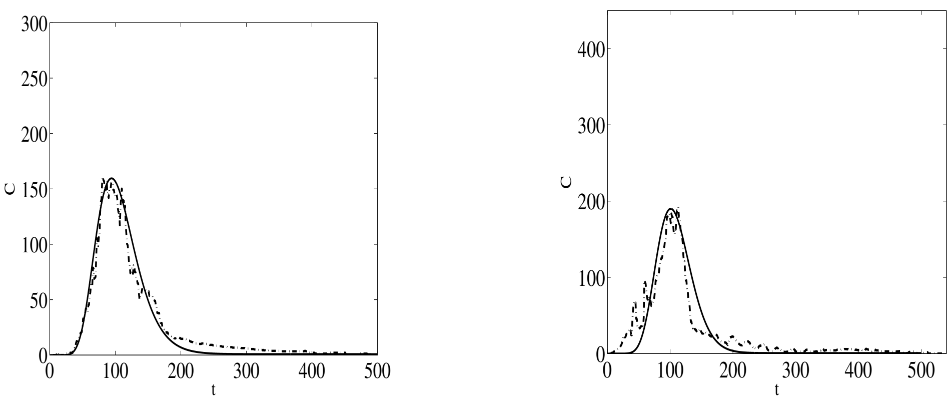

FIGURE 4. Numerical Solution (−); Experimental results (−·−): (a) I.P8 (b) II.P8

Solute concentration, C_s, in storage zones

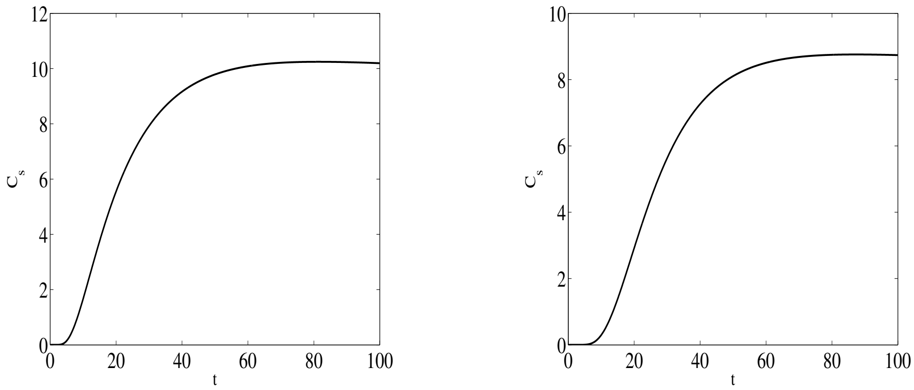

FIGURE 5. Numerical Solution (−): (a) I.P2 (b) II.P2

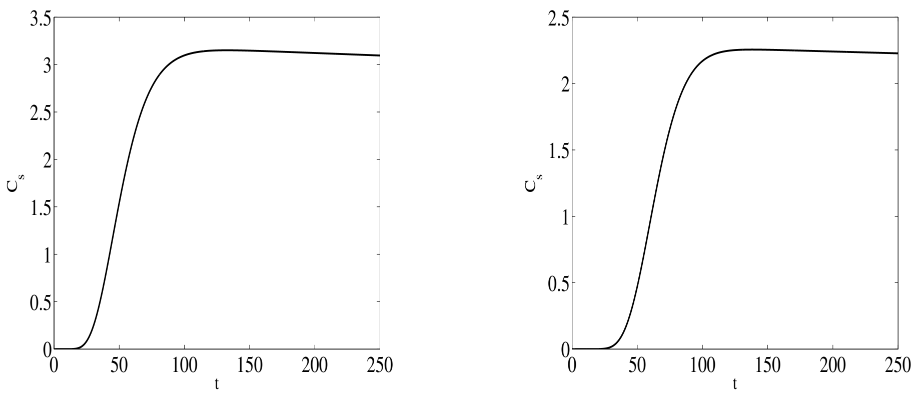

FIGURE 6. Numerical Solution (−): (a) I.P5 (b) II.P5

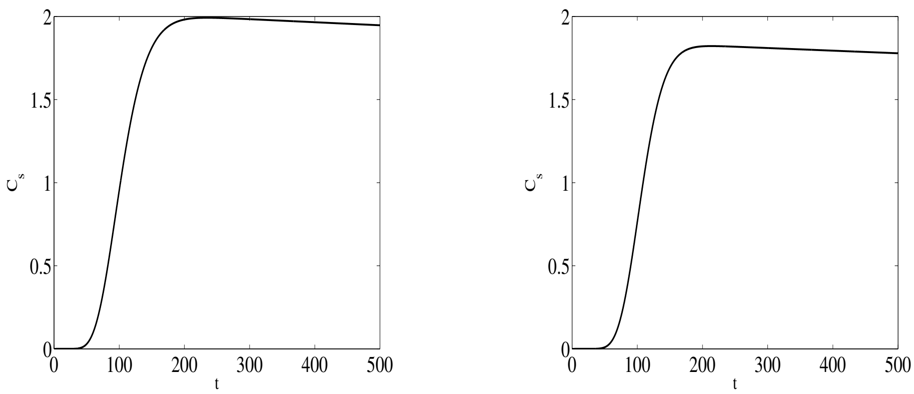

FIGURE 7. Numerical Solution (−): (a) I.P8 (b) II.P8